

Extra EPR Spectra of Iron-Doped Rutile

Per-Olof Andersson and Erik L. Kollberg
Research Laboratory of Electronics, Göteborg, Sweden

Andrzej Jelenski
Institute of Electron Technology, Warsaw, Poland
 (Received 24 May 1973)

We have discovered that besides the well-known EPR spectrum of Fe^{3+} substitutional ions in iron-doped rutile there are several other EPR spectra related to Fe^{3+} ions. The interpretation of these extra spectra was made considering the intensity variation with heat treatment and the orientation of the magnetic axes of the extra spectra. Isofrequency diagrams were recorded at 9.2 GHz and isogon plots were measured up to 62 GHz. One extra spectrum, spectrum I, was found to have zero-field splittings (ZFS) of 32.1 and 50.7 GHz. Spectrum I could be described by the spin-Hamiltonian parameters $D = 13.1$ GHz, $E = 2.3$ GHz, $a = -0.7$ GHz, $F = 1.9$ GHz, $g_x = 1.993$, $g_y = 2.040$, and $g_z = 1.998$. We interpret spectrum I as due to a substitutional Fe^{3+} ion which is perturbed by a proton nearby. The position of this proton in the lattice is determined. Another spectrum, spectrum II, has one ZFS of 61.4 GHz. The other ZFS is expected around 81.6 GHz but could not be observed because of lack of a signal source. Spectrum II could be described by the following approximate spin-Hamiltonian parameters: $D = 22.9$ GHz, $E = 2.7$ GHz, $a = -0.1$ GHz, $F = 6.3$ GHz, $g_x = 2.001$, $g_y = 1.993$, and $g_z = 2.001$. We interpret spectrum II as due to a substitutional Fe^{3+} ion that is perturbed by a nearest-neighbor oxygen vacancy. Several lines of a third spectrum were also identified and tentatively interpreted as due to a substitutional Fe^{3+} ion with a Ti^{4+} interstitial ion nearby. Further weak spectra were seen but could not be given any definite interpretation.

I. INTRODUCTION

It is well known¹ that most of the iron in iron-doped rutile (TiO_2) substitutes for Ti^{4+} ions as Fe^{3+} . Therefore the difference in charge in the crystal has to be compensated by the introduction of defects such as oxygen vacancies and different types of interstitial ions. This has been observed in chromium-doped rutile, where EPR spectra have been found that are related to Cr^{3+} substitutional ions associated with second- and third-neighbor oxygen vacancies.² In cobalt-doped rutile EPR spectra from cobalt ions that were associated with oxygen vacancies³ and titanium interstitials⁴ were found. Similar measurements have been reported for SrTiO_3 doped with chromium⁵ and with iron.^{6,7} No similar measurements on iron-doped rutile, however, have been reported until now. Heat treatment has here been used (see also Ref. 8) as an efficient tool to interpret and identify EPR spectra associated with defects.

II. GENERAL DISCUSSION

A. Spin-Hamiltonian Operator

An EPR spectrum related to an $S = \frac{5}{2}$ system without hyperfine splitting, such as Fe^{3+} , may be described quantum mechanically by the following spin-Hamiltonian operator¹:

$$\begin{aligned} \bar{H} = & (g\mu_B/h)\bar{\mathbf{B}} \cdot \bar{\mathbf{S}} + D(S_x^2 - \frac{35}{12}) + E(S_x^2 - S_y^2) \\ & + \frac{1}{6}a(S_x^4 + S_y^4 + S_z^4 - \frac{707}{16}) + \frac{7}{36}F(S_x^4 - \frac{95}{14}S_x^2 + \frac{81}{16}), \end{aligned}$$

where $\bar{\mathbf{S}}$, S_x , S_y , and S_z are spin operators and g , D , E , a , and F are the experimentally determined spin-Hamiltonian parameters. When these are known, energy levels and transition probabilities are readily calculated.

The strongest EPR spectrum which can be observed in iron-doped rutile is related to substitutional Fe^{3+} ions with no perturbation nearby. We will call this spectrum the "main spectrum." The spin-Hamiltonian parameters of the main spectrum are¹

$$\begin{aligned} D &= 20.35 \pm 0.1 \text{ GHz}, \quad E = 2.21 \pm 0.07 \text{ GHz}, \\ a &= 1.1 \pm 0.2 \text{ GHz}, \quad F = 0.5 \pm 0.3 \text{ GHz}, \\ g &= 2.000 \pm 0.005. \end{aligned}$$

All other EPR spectra will be called "extra spectra." They may be related to substitutional Fe^{3+} ions with a lattice defect nearby, to substitutional ions other than Fe^{3+} , to interstitial ions, and to various paramagnetic complexes and clusters of Fe^{3+} ions such as pairs, triads, etc.

B. Symmetry Considerations

From the crystalline symmetry, there are two magnetically nonequivalent lattice sites at P_I and P_{II} (Fig. 1). We will consider a paramagnetic ion in a crystal field with the same symmetry as at P_I and P_{II} as belonging to the magnetic complexes I and II, respectively. Complex I differs from complex II only by a rotation of 90° around the c axis

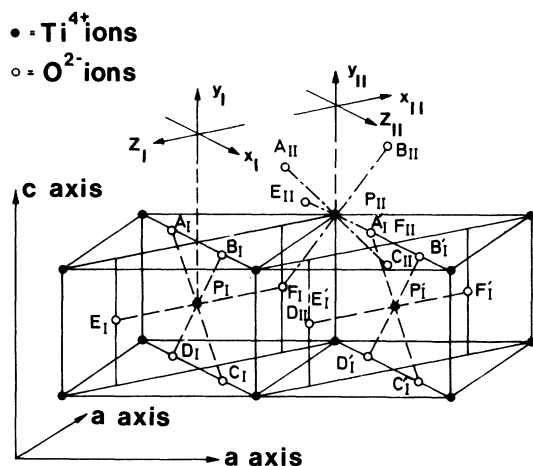


FIG. 1. Crystal structure and axis definitions of rutile (TiO_2).

(both complexes are described with the same spin-Hamiltonian parameters). There will be an equal number of ions in each of the two complexes.

Now consider the coordinate system (x_I, y_I, z_I) with the origin at the site of the substitutional P_I in Fig. 1 and with the coordinate axes along the crystalline directions $[\bar{1}\bar{1}0]$, $[00\bar{1}]$, and $[\bar{1}\bar{1}0]$. Let us assume perturbations to exist in the lattice, changing the EPR spectrum of the substitutional Fe^{3+} ion. Let a perturbing lattice defect be located at a certain position, for example, at x_{10}, y_{10}, z_{10} . Since the $x_I y_I, x_I z_I$, and $y_I z_I$ planes are all reflection planes, equivalent defect sites are found by the changing sign for one, two, or all three of the coordinates x_{10}, y_{10} , and z_{10} . Hence there are for one complex eight equivalent defect sites. However, perturbations at (x_{10}, y_{10}, z_{10}) and $(-x_{10}, -y_{10}, -z_{10})$ are not distinguishable in EPR experiments, since the resulting magnetic coordinate systems are identical.

Hence, since there are two nonequivalent substitutional sites (P_I and P_{II}) in the regular lattice, we may distinguish a maximum of eight different magnetic complexes for a certain extra spectrum. When the static magnetic field is applied along any of the magnetic axes of the main spectrum (the x_I, y_I , or z_I axis) the energy-level diagrams of paramagnetic ions at the P_I sites, perturbed by equivalent lattice defects, become identical. In the same way the energy-level diagrams of perturbed P_{II} ions will be equal for the static magnetic field along the magnetic axes of the main spectrum (x_{II}, y_{II}, z_{II}).

Thus for the same transition we will observe a maximum of two absorption lines with the magnetic field aligned along the x_I, z_{II} axis and z_I, x_{II} axis, respectively. For the magnetic field along the c

axis (magnetic y axes of spectrum I and II) however, we will observe only one absorption line per transition. When the static magnetic field deviates from any xz, xy , or zy plane, a maximum of eight absorption lines per transition, four from each of the perturbed P_I and P_{II} sites, may be observed.

III. MEASUREMENTS

EPR measurements were performed at 9.2 GHz using a Varian EPR spectrometer, type E-3. With the static magnetic field along the c axis, the main spectrum and the extra-spectra absorption lines were recorded for all samples. A low-resolution recording for an Fe^{3+} -doped-rutile crystal with the static magnetic field along the c axis is shown in Fig. 2. The multitude of extra EPR lines is clearly demonstrated. The areas of these absorption lines were obtained by integrating the recorded derivatives twice. For the weaker lines and in a few cases for stronger lines, the areas were estimated by assuming Gaussian line shape. The static magnetic field was then turned in the main spectrum $ac, x_I c, z_I c$, and aa planes and the isofrequency diagrams depicted in Fig. 3-7 were recorded (note that the well-known main EPR spectra of Fe^{3+} and Cr^{3+} ions are omitted).

We also measured EPR spectra for various frequencies between 4 and 62 GHz at 4.2 °K and with the static magnetic field aligned along the TiO_2 c axis (Figs. 8 and 9). For frequencies between 4 and 12 GHz we used a coaxial line formed by two coaxial stainless-steel tubes with a large piece of single-crystalline $\text{TiO}_2 : \text{Fe}$ close to the short-circuited end. The $\text{TiO}_2 : \text{Fe}$ crystal formed a large dielectric resonator with a high-internal- Q value. Resonance frequencies were found with an average spacing of 300 MHz. A magnetic field modulation of 25 Hz (half the ac line frequency) and a lock-in amplifier were used. The high- Q value of the dielectric resonator, the large filling factor, and liquid-helium temperatures ensured a high sensitivity.

The EPR spectrum from 18-62 GHz was measured using a large piece of single-crystalline $\text{TiO}_2 : \text{Fe}$ placed in a stainless-steel K -band waveguide. Since the resonances were close in frequency and since the high- Q values yielded a very good sensitivity, measurements at almost any frequency could easily be made. Since the sensitivity increases as the frequency squared, no magnetic field modulation was required and only a crystal detector and an oscilloscope for detecting the absorption lines were needed.

Some extra EPR transitions associated with the same paramagnetic centers could be identified by the use of a double-resonance technique. Extra lines were monitored by applying a signal frequency somewhere between 5 and 9 GHz. At the same

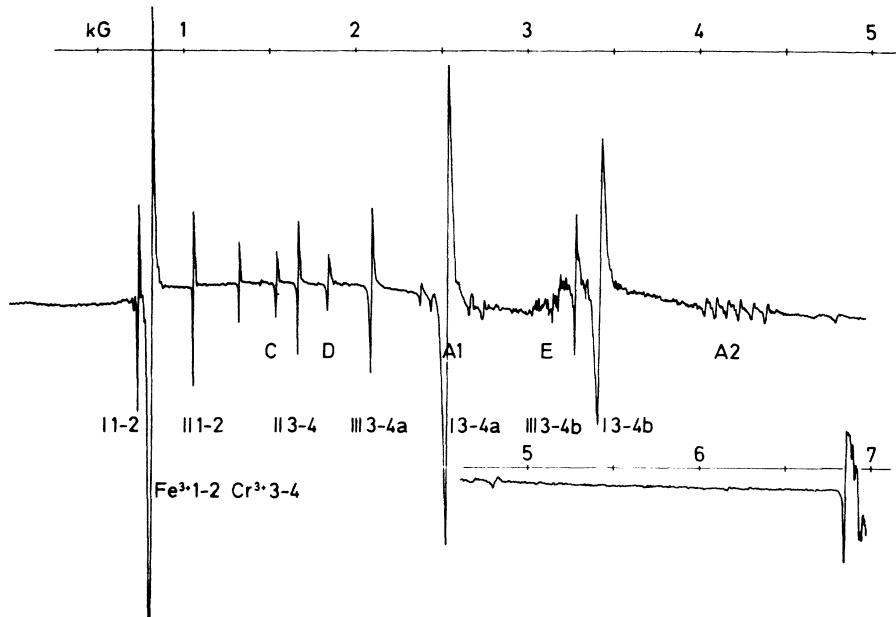


FIG. 2. Example of an EPR recording of an iron-doped sample at 9.2 GHz. The magnetic field is oriented along the *c* axis.

time, a "pump" frequency between 42 and 62 GHz was applied and the frequencies, where increased absorption (antimaser action) or inversion (maser action) at the signal transition were obtained, are

plotted in Fig. 9. Another important means of identifying different EPR spectra were the changes in intensities of the different spectra that occurred on heat treatment.

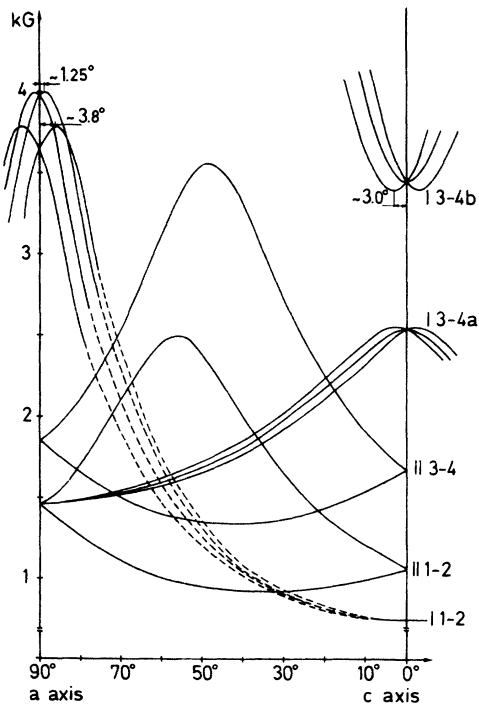


FIG. 3. Isospectrum diagram of spectrum I and spectrum II in the *ac* plane, $f=9.2$ GHz.

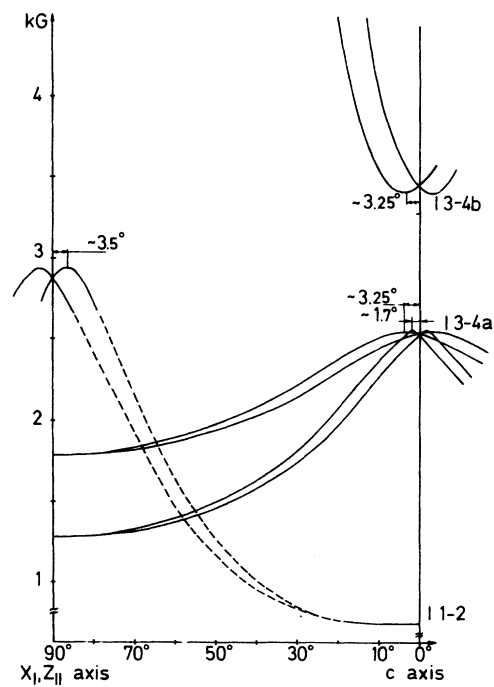


FIG. 4. Isospectrum diagram of spectrum I in the x_1c , $z_{11}c$ plane, $f=9.2$ GHz.

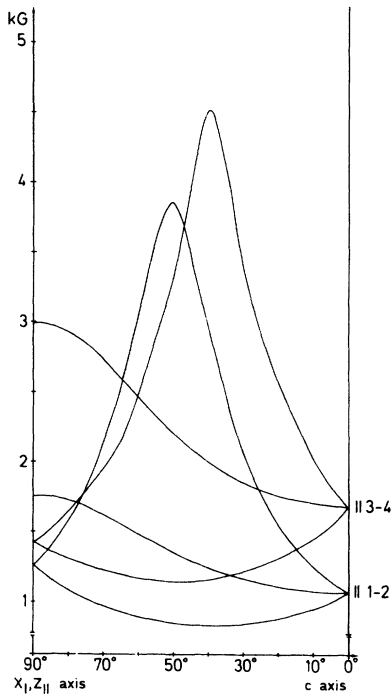


FIG. 5. Isofrequency diagram of spectrum II in the x_1c, z_1c plane, $f=9.2$ GHz.

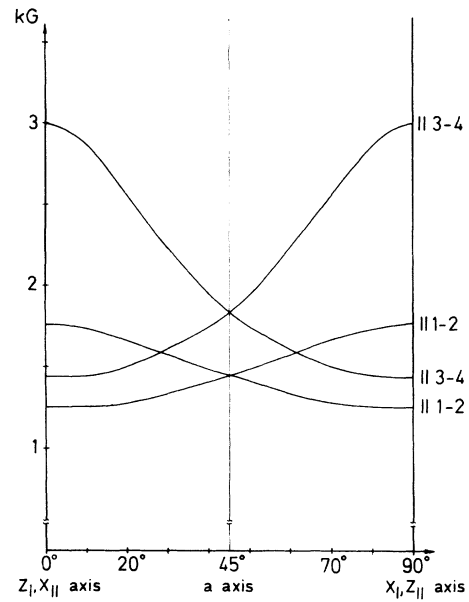


FIG. 7. Isofrequency diagram of spectrum II in the aa plane, $f=9.2$ GHz.

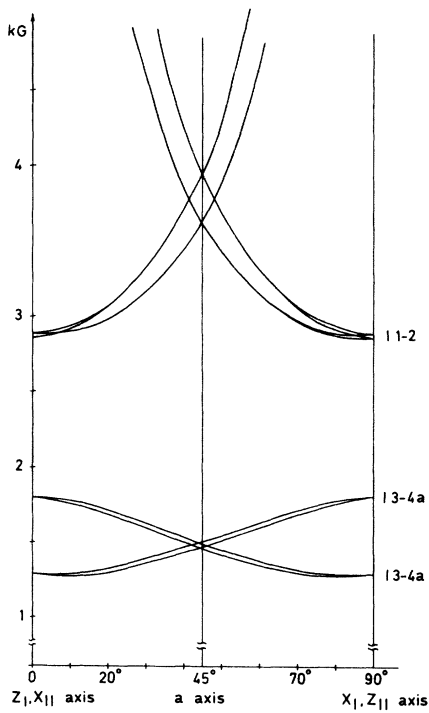


FIG. 6. Isofrequency diagram of spectrum I in the aa plane, $f=9.2$ GHz.

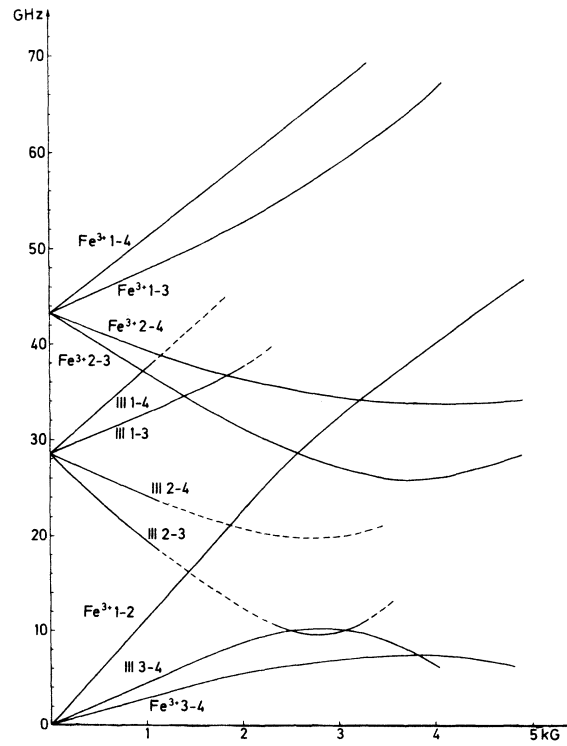


FIG. 8. Isogon plot of the main spectrum and spectrum III for the magnetic field along the c axis.

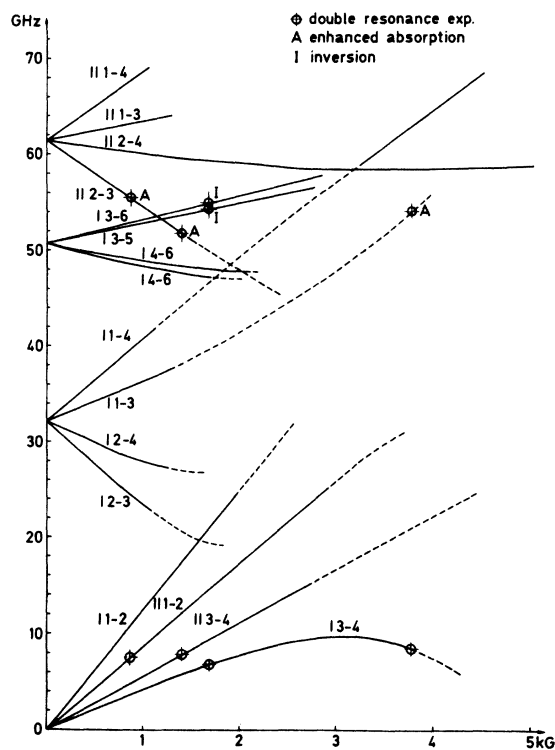


FIG. 9. Isogon plot of spectrum I and spectrum II for the magnetic field along the c axis. Solid lines are obtained from EPR absorption measurements while broken lines are extrapolated.

IV. SPECTRUM I

A. Identification

This spectrum was easy to separate in the recordings at 9.2 GHz since the intensities of the absorption lines belonging to this spectrum were very sensitive to heat treatment. The intensities decreased on quenching and increased on annealing. Identification of the high-frequency transition of spectrum I (see Fig. 9) was done by observing the proposed I 3-4 transition at 1660 G with the static magnetic field aligned along the c axis. Then we were able to invert this absorption line by applying pump power at 54.2 GHz (3-5 transition) and 54.7 GHz (3-6 transition). Furthermore, the absorption from the I 3-4 transition at 8.8 GHz and 3800 G was increased by pumping the I 3-4 transition at 54.3 GHz. It was also possible to identify the Kramer's doublet transitions I 1-2, I 3-4, and I 5-6 by calculating the difference between the "pump" transitions. The small splitting of the I 5-6 transition is expected in the $S = \frac{5}{2}$ spin system with the static magnetic field aligned along the y axis.

B. Orientation

A determination of the orientations of the magnetic coordinate systems of spectrum I was made by

considering the symmetry properties observed in the isofrequency diagrams (Figs. 3, 4, and 6).

The angles to the maxima in magnetic field in the $x_{I,II}c$, $z_{I,II}c$, and ac planes from the $x_{I,II}$, $z_{I,II}$, and a axes, respectively, indicated that the direction of the magnetic $y'_{I,II}$ axis (primed coordinate system) is related to the magnetic axes of spectrum I) can be found by rotating the $y_{I,II}$ axis approximately 4° around an axis in the aa plane, 27° off the $z_{I,II}$ axis.

The deviation of the maxima in magnetic field from the c , a , $x_{I,II}$, and $z_{I,II}$ axes, respectively (see Figs. 3 and 4), are caused by the tilt of $\pm 4^\circ$. However, this small tilt means that the new axes $x'_{I,II}$, $y'_{I,II}$, $z'_{I,II}$ move out of the ac , $x_{I,II}c$, and $z_{I,II}c$ planes only about 0.1° . The tilt alone cannot then explain the fact that there is a difference in the maximum magnetic fields at 1.25° and 3.8° , respectively, from the a axis in the ac plane (see Fig. 3). A rotation of about 2° around the c axis is necessary to explain this feature.

Using a computer program, we found a best fit to experimental data for an orientation of the coordinate system x', y', z' obtained by performing the following operations on the coordinate system x, y, z : (i) a rotation around the TiO_2 c axis with about $\alpha = \pm 2.0^\circ$; (ii) a rotation of $\beta = \pm 3.7^\circ$ around an axis in the ab plane at an angle of $\gamma = 26.1^\circ$ to the z axis.

For the two nonequivalent sites P_I and P_{II} in Fig. 1, we obtain a set of eight possible nonequivalent orientations for the magnetic coordinate systems of spectrum I. All the eight spectra related to the eight magnetic complexes have been observed experimentally when the magnetic field is oriented out of the xc , zc , and ac planes of the main spectrum. A more extensive discussion on details in the isofrequency diagram can be found in Ref. 8.

The isofrequency diagram of spectrum I in the $x'_I y'_I$ and $z'_{II} y'_{II}$ planes is shown in Fig. 10. Here the magnetic field at the extrema in the $x_I y_I$ and $z_{II} y_{II}$ planes have been assumed equal to the extrema in the $x'_I y'_I$ and $z'_{II} y'_{II}$ planes. This is not entirely correct but the error should be small as the orientation of the coordinate system x'_I, y'_I, z'_I differs only slightly from that of the main spectrum coordinate system x_I, y_I, z_I .

C. Determination of Spin-Hamiltonian Parameters

From Fig. 9 the zero-field splittings of spectrum I are

$$f_{13} = 32.1 \text{ GHz}, \quad f_{15} = 50.7 \text{ GHz}.$$

The spin-Hamiltonian parameters describing spectrum I were found by fitting the parameters using a computer program to a number of experimentally determined resonance frequencies and magnetic fields at various angles of the static magnetic field.

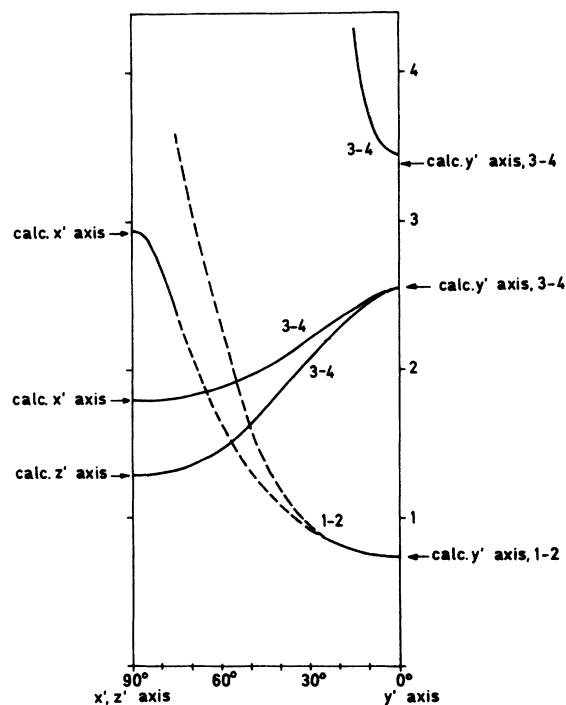


FIG. 10. Isfrequency diagram of spectrum I in the $x'_1y'_1$ and $z'_1y'_1$ plane.

The final values used are (in GHz)

$$g_x = 1.993, \quad D = 13.1, \quad a = -0.7,$$

$$g_y = 2.040, \quad E = 2.3, \quad F = 1.9,$$

$$g_z = 1.998.$$

Using these spin-Hamiltonian parameters, transition probabilities were calculated for the static magnetic field parallel to the c axis and for the rf field linearly polarized along the a axis (as in the experiments performed in the Varian spectrometer at 9.2-GHz), we obtained relative measures for the transition probabilities⁹ as shown in Table I.

The intensity ratio between the 1-2 and the 3-4 transitions is predicted as 0.22 which may be compared to the measured values 0.14. An even better agreement, however, was obtained for the 3-4 transitions at 2533 and 3420 G, where we measured

the ratio 1.06 compared to the theoretical value 1.15. The discrepancy between theory and experiments for the intensity ratio of the 1-2 and 3-4 transitions may be explained by experimental errors, partly due to the small intensity of the 1-2 transition and by the error in our determination of spin-Hamiltonian parameters. The agreement between theory and experiment is quite good however, which supports the choice of the values for the spin-Hamiltonian parameters.

D. Interpretation of Spectrum I

A linear relation between the intensity of spectrum I and the infrared OH line at 3286 cm^{-1} was observed.^{8,10} We found that when the samples were heated in ordinary commercially available oxygen gas, the intensity of the infrared OH line and spectrum I decreased upon quenching and increased upon annealing. However, upon annealing in an oxygen atmosphere carefully cleaned from hydrogen and water vapor, both spectra almost disappeared. Therefore spectrum I can be interpreted as due to a substitutional Fe^{3+} ion which is perturbed by an interstitial proton nearby.

E. Position of the Proton in the Rutile Lattice

The position of the proton in the rutile lattice has not been conclusively established before. The orientation of the magnetic coordinate system of spectrum I with respect to the crystalline axes of rutile gives a clear indication of the position of the proton.

Earlier, Von Hippel *et al.*¹¹ suggested after Pimentel and McClellan that the frequency shift from the value for the free OH ion indicates an O-H-O distance of about 2.75 \AA . This corresponds to the distance between the oxygen atoms denoted E_1 and F_1 and the four oxygen atoms A_1 , B_1 , C_1 , and D_1 in the elementary cell (Fig. 1). Data collected by these authors also show that the proton should be placed approximately at 1 \AA from one of the oxygen atoms. Soffer¹² found that this OH absorption band was dichroic, with an absorption coefficient more than 7 times greater when the electric field vector is applied in the direction of the a axis, than in the c -axis direction. This was explained by Von Hippel as due to a screening effect

TABLE I. Transition probabilities of spectrum I with the static magnetic field aligned along the c axis, $f=9.20 \text{ GHz}$.

Transition	Experimental magnetic field (G)	Theoretical transition frequency (GHz)	Transition probability σ^2
1-2	737	9.45	0.21
3-4	2533	9.18	1.04
3-4	3420	9.12	0.90

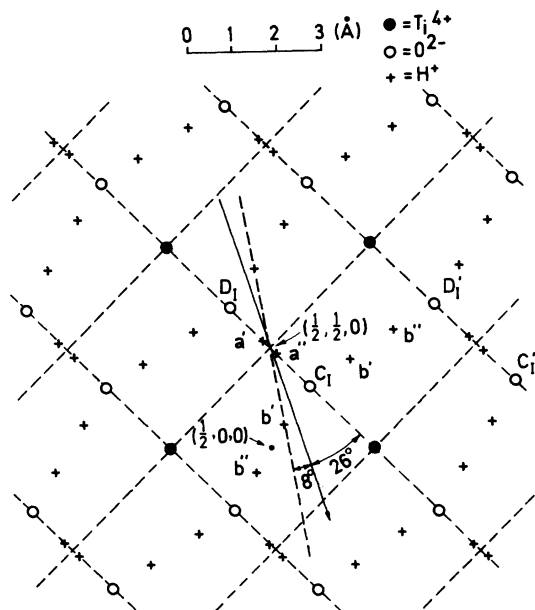


FIG. 11. Positions of the proton in the basal (aa) plane of rutile. Dotted lines mark the channels of easy diffusion. The Fe^{3+} ion is situated at $(\frac{1}{2}, \frac{1}{2}, 0)$.

of the protons in the c -axis direction. Johnson *et al.*¹³ found that the dichroism was larger than 99%. Hill¹⁴ measured the ratio of absorption of unpolarized light incident in the c -axis direction to the light incident in the a -axis direction to be 2.06, close to the value 2 calculated for OH bonds in the aa plane and contrary to the value 1.61 calculated for the proton sites suggested by Von Hippel *et al.*¹¹ This shows that the proton is situated in the aa plane (the basal plane). The possible sites for protons in this plane are shown in Fig. 11.

Hill indicates that the bonds should be between D_1 and C_1 or D_{11} and C_{11} , etc. Since the distance between these oxygen atoms is 2.52 Å and the OH distance according to Pimentel and McClellan¹⁵ is 1.06 Å, this will give two possible sites a' and a'' for the proton. But in this case, also according to Pimentel and McClellan, the frequency shift from the value 3700 cm^{-1} for the unassociated OH^- ion should be $\sim 1000 \text{ cm}^{-1}$ thus giving a line frequency of ~ 2700 and not 3286 cm^{-1} as observed. Another possible site is between the C_1 and D'_1 oxygen atoms (see Fig. 11). Since the distance between C_1 and D'_1 is about 3.3 Å, one may expect after Pimentel that the protons should be at the positions b' and b'' , about 0.96 Å from the oxygen atoms. Moreover, the frequency should be nearly equal to the value of the unassociated OH^- ion. Also, the C_1 and D'_1 oxygen atoms lie on both sides of the open channel of easy diffusion, thus increasing the prob-

abilities of occupation of these sites.

Johnson *et al.*¹³ also discuss the two possible sites for a proton at approximately $(\frac{1}{2}, 0, 0)$ and $(\frac{1}{2}, \frac{1}{2}, 0)$ (see Fig. 11). Johnson gives the following argument for the $(\frac{1}{2}, 0, 0)$ site to be preferred. The OH separation distance in various crystals typically lies in the range 1.0–1.15 Å, depending only weakly on the crystalline field. The distance between the C_1 and D_1 ions is 2.52 Å and hence the proton at $(\frac{1}{2}, \frac{1}{2}, 0)$ should approach either the C_1 or D_1 oxygen ion. The proton then experiences a double-well potential rather than a simple harmonic one. The second potential minimum will essentially cause a splitting of more than 100 cm^{-1} of the OH line, which is not observed.

In Fig. 11 the direction of the projection on the basal plane of the magnetic y' axes of spectrum I is plotted. The deviation of this projection line from the direction of the proton (with an OH distance of 1.0–1.15 Å) is 8° towards the main spectrum x_1 axis. It also shows that the preferred proton position (0.56, 0.11, 0) that gives rise to one spectrum I complex is the one that is closest to the Fe^{3+} ion at $(\frac{1}{2}, \frac{1}{2}, \frac{1}{2})$.

The symmetry of spectrum I thus shows, that for an Fe^{3+} ion at a substitutional $(\frac{1}{2}, \frac{1}{2}, \frac{1}{2})$ site, the protons are positioned at approximately $(\frac{1}{2}, 0, 0)$ and equivalent sites. The site $(\frac{1}{2}, \frac{1}{2}, 0)$ is completely ruled out by the symmetry of spectrum I, Johnson's suggestion¹³ that for the Fe^{3+} ion at (0, 0, 0) the proton occupies the $(\frac{1}{2}, 0, 0)$ sites, is also ruled out by the symmetry of spectrum I.

V. SPECTRUM II

A. Identification

The identification of spectrum II was facilitated by the fact that for this spectrum the intensity was increased upon quenching. In Fig. 12 the isofrequency diagram of spectrum II at 9.2 GHz in the x_1y_1 , z_1y_1 , and aa planes of the main spectrum is depicted, as obtained from Figs. 3, 5, and 7. The magnetic axes of spectrum II for each of the lattice sites P_1 and P_{11} (Fig. 1) are found by simply rotating the main spectrum coordinate system 90° around the y axis and 40° around the z axis (see Fig. 13). In Fig. 14 spectrum II is shown using its own magnetic axes (x'' , y'' , z'') and for one of the two non-equivalent substitutional sites of the TiO_2 lattice. Using the double-resonance technique, we were able to identify one zero-field splitting of spectrum II at 61.4 GHz (Fig. 9). For a static magnetic field of 880 G the II 2-3 transition was pumped at 55.5 GHz, yielding an enhanced absorption for the observed II 1-2 transition (7.8 GHz). Moreover, for a static magnetic field of 1250 G, we were able to pump the II 2-3 transition at 51.8 GHz, observing increased absorption for the II 3-4 transition (7.8

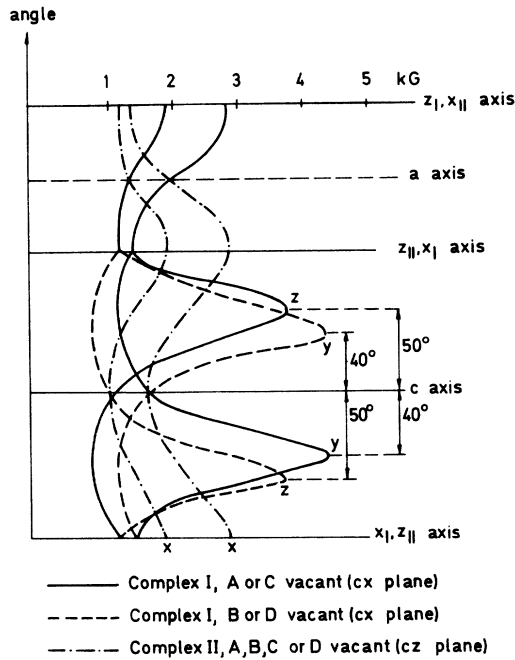


FIG. 12. Isofrequency diagram of spectrum II in the aa and x_{1c} , z_{11c} planes.

GHz). The frequencies of the II 1-2 and II 3-4 transitions can then be calculated as the frequency differences $f_{14} - f_{13} = f_{23} - f_{24} = f_{34}$ and $f_{14} - f_{24} = f_{13} - f_{23} = f_{12}$. The II 1-2 and II 3-4 transitions were separated by observing the faster increase of the intensity of the II 1-2 transition with decreasing temperature at liquid-helium temperatures.

However, only one zero-field splitting was observed in the frequency interval 3-62 GHz. The other zero-field-splitting frequency is then probably larger than 62 GHz.

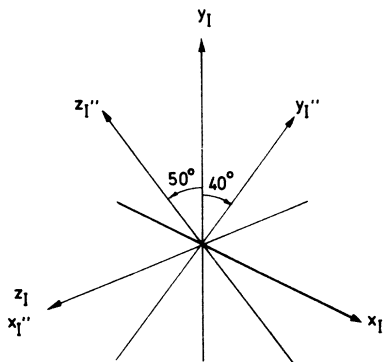


FIG. 13. Magnetic axes of complex I of the main Fe^{3+} spectrum (x_1 , y_1 , z_1) and magnetic axes of complex I of spectrum II (x_1' , y_1' , z_1').

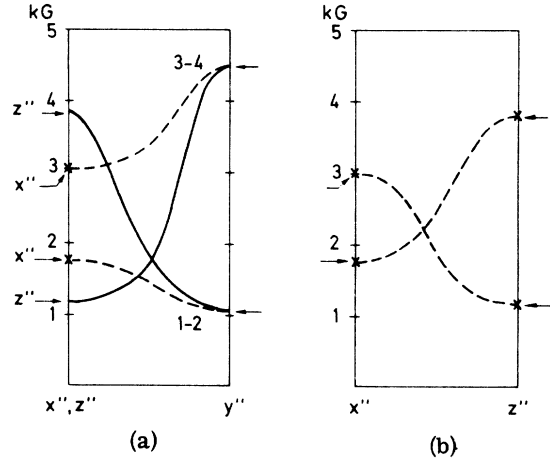


FIG. 14. Isofrequency diagram of spectrum II in its own magnetic coordinate system (x'' , y'' , z'') and for one of the two nonequivalent substitutional sites of the TiO_2 lattice. (a) shows the $x''y''$, $z''y''$ plane and (b) the $x''z''$ plane.

The spin-Hamiltonian parameters were fitted by the help of a computer program as for spectrum I. We found (in GHz)

$$\begin{aligned} g_x &= 2.001, & D &= 22.9, & a &= -0.1, \\ g_y &= 1.993, & E &= 2.7, & F &= -6.3, \\ g_z &= 2.001. \end{aligned}$$

The second zero-field splitting then becomes 81.6 GHz. The transition probabilities obtained with these data are given in Table II. The static magnetic field is aligned along the c axis of the rutile and the linearly polarized rf magnetic field is directed along the rutile a axis. However, these transition probabilities do not fit the experimental evidence $\sigma_{12}^2/\sigma_{34}^2 = 1.13$. This discrepancy is probably due to the lack of data on the second zero-field-splitting frequency, giving an inadequate fit of the spin-Hamiltonian parameters.

B. Interpretation of Spectrum II

Spectrum II can be interpreted as due to an oxygen vacancy at $A_{1,II}$, $B_{1,II}$, $C_{1,II}$, or $D_{1,II}$ (Fig. 1). This interpretation is supported by the symmetry properties of the EPR spectrum shown in Figs. 12-

TABLE II. Transition probabilities of spectrum II with the static magnetic field aligned along the c axis, $f = 9.20$ GHz.

Transition	Experimental magnetic field (G)	Theoretical transition frequency (GHz)	Transition probability σ^2
1-2	1062	9.27	0.46
3-4	1667	9.29	0.14

14, where the magnetic y'' axis is directed 40° off the c axis exactly in the direction P_1-A_1 , etc.

Another evidence for the interpretation of spectrum II as due to oxygen vacancies is the fact that quenching, which slightly reduces the crystal and creates oxygen vacancies, also increases the intensity of spectrum II. Annealing, on the contrary, reduces the intensity of this oxygen-vacancy-defect spectrum.

It is quite interesting to make a comparison with $\text{TiO}_2:\text{Cr}$. The extra spectra² of $\text{TiO}_2:\text{Cr}$ are associated with second- and third-neighbor oxygen vacancies. No extra spectrum related to nearest-neighbor oxygen vacancies is observed. Furthermore, the introduction of hydrogen does not create any spectrum similar to spectrum I of $\text{TiO}_2:\text{Fe}$. Similar results have been reported for iron- and chromium-doped SrTiO_3 . For $\text{SrTiO}_3:\text{Fe}$, Kirkpatrick *et al.*⁶ and Baer *et al.*⁷ discovered an EPR spectrum associated to substitutional Fe^{3+} ions with nearest-neighbor oxygen vacancies, as we have found for $\text{TiO}_2:\text{Fe}$. The oxygen vacancies of $\text{SrTiO}_3:\text{Cr}$, however, are according to Meierling⁵ located outside the oxygen octahedron surrounding the chromium ion.

VI. SPECTRUM III

It was not possible to determine the isofrequency diagram of this spectrum, since it is quite weak compared with other extra-spectrum absorption lines. One zero-field splitting related to spectrum III is found at 28.6 GHz (see Fig. 8). Transition 1-2 cannot be observed, since it probably coincides with the 1-2 transition of the main spectrum. The Kramer's doublet which is observed in Fig. 8 has the general shape of a 3-4 transition for an $S = \frac{5}{2}$ system with the static magnetic field directed along the magnetic y axis. This indicates that the transition probability at 9.2 GHz is of the order $\sigma^2 \approx 1$ (compare the transition probability of the main spectrum $\sigma^2 \approx 1.0-1.2$ and the transition probability of spectrum I).

The increase of the amplitude with time of heat treatment seems to exclude the possibility that the spectrum is related to complexes formed by substitutional iron ions and second- or third-neighbor oxygen vacancies. Since substitutional iron seems to attract positive lattice defects such as oxygen vacancies and H^+ interstitials, spectrum III might be due to complexes formed by an iron ion with a (slowly diffusing) Ti^{4+} interstitial nearby. It may be interesting to note that Miyako⁴ in $\text{TiO}_2:\text{Co}^{2+}$ found an extra spectrum caused by substitutional Co^{2+} ions associated with Ti^{4+} interstitials. However, no conclusive interpretation of spectrum III is possible, mainly due to the lack of complete isofrequency diagrams.

VII. SOME ADDITIONAL EXTRA-SPECTRUM TRANSITIONS OBSERVED

Additional extra-spectrum absorption lines were observed with the 9.2-GHz EPR spectrometer (see Fig. 2). Spectrum A was only observed in samples originating from one particular boule and was not observed in undoped samples. A possible interpretation may be that spectrum A is caused by Mn^{2+} which to 100% has a nuclear spin of $\frac{5}{2}$. Another possibility is that spectrum A is associated with Al^{3+} ions (also nuclear spin of $\frac{5}{2}$), forming paramagnetic centers with Fe^{3+} . Spectrum B, C, D, and E in Fig. 2 do not seem to be related to the same structure. Spectrum E seems to be independent of Fe^{3+} concentration and heat treatment. From measurements at different frequencies, spectrum E has been proved to be a Kramer's doublet, with a g factor of about 2.08. Spectrum B coincides with the 1-2 transition of spectrum II for the c -axis orientation. Hence, this spectrum must be measured off the c axis.

Finally there is a very broad line (~ 200 G) at a field of 3250 G yielding a g factor of about 2.0 which is quite isotropic. The surface of the absorption line is quite large, and in most cases many times larger than the main-spectrum iron line. This line is probably caused by trapped electrons and exists in all crystals including the undoped ones.

VIII. CONCLUSIONS

In the complicated EPR spectrum of iron-doped rutile we have identified four characteristic spectra. There are further EPR lines that possibly may be grouped and thereafter also interpreted. However, we found it impossible to do this from our experimental data. For the three more complete spectra, the data for two of them allowed for a firm interpretation. One spectrum is clearly associated with proton interstitials nearby Fe^{3+} substitutional ions. The symmetry for this spectrum shows that for the iron at the position $(\frac{1}{2}, \frac{1}{2}, \frac{1}{2})$, the proton may occupy any of the eight sites $(\frac{1}{2}, 0, 0)$, $(0, \frac{1}{2}, 0)$, $(1, \frac{1}{2}, 0)$, $(\frac{1}{2}, 1, 0)$, $(\frac{1}{2}, 0, 1)$, $(0, \frac{1}{2}, 1)$, $(1, \frac{1}{2}, 1)$, and $(\frac{1}{2}, 1, 1)$. On annealing at a high temperature (1200 °C), a substantial number of the protons leave the crystal. Hence, a rapid cooling from 1200 °C yields crystals with a small content of protons. If the crystal is cooled slowly (≈ 50 °C/h), protons successively get trapped in the crystal and no more protons will leave the crystal. If the surrounding gas contains small amounts of hydrogen or water vapor, we will now get a net flow of protons into the crystal from the surrounding atmosphere. Hence, spectrum I is more intense in annealed crystals than in quenched ones due to the excess number of protons. If, however, the crys-

tal is annealed in an oxygen gas carefully cleaned from hydrogen and water vapor, there will be few protons in the lattice irrespectively of the cooling rate and spectrum I is very weak.

Spectrum II is associated with an Fe^{3+} substitutional ion having an oxygen vacancy as a nearest neighbor. This spectrum is most intense in crystals rapidly cooled from 1200 °C, since at this high temperature the crystal is in a reduced state. A slow cooling, however, reduces the intensity of spectrum II which of course means that oxygen is again captured by the crystal at lower temperatures. These conclusions are in excellent agreement with the results.

The interpretation of a third spectrum, spectrum III, is less certain mainly due to lack of experimental data. However, we suggest that this spectrum is due to substitutional Fe^{3+} ions, having a Ti^{4+} interstitial ion nearby.

The discovery and our interpretation of spectra I, II, and III, as well as the results^{2,5-7} on $\text{TiO}_2:\text{Cr}$, $\text{SrTiO}_2:\text{Cr}$, and $\text{SrTiO}_3:\text{Fe}$ support the crystal-field calculations for Fe^{3+} and Cr^{3+} ions with high-spin and low-spin configurations in an octahedral neighborhood subjected to distortions

(Schläfer¹⁶). These calculations show that for a distortion caused by the removal of a ligand, the total energy of an Fe^{3+} ion remains constant, while the total energy of a Cr^{3+} ion increases. These results are also in agreement with reaction kinetic investigations (Schläfer¹⁶), indicating that in comparison with other metal complexes of the first transition series octahedral Cr^{3+} complexes are most stable against exchange and removal of ligands. The relative abundance of further extra EPR lines (C, D, and E in Fig. 2) compared to what is found in $\text{TiO}_2:\text{Cr}$ may also be due to the fact that Fe^{3+} substitutional ions attract positive impurities and lattice defects. In a subsequent paper¹⁰ the results reported above will be used for a discussion of charge-compensation mechanisms.

ACKNOWLEDGMENTS

We are indebted to Dr. R. Aasa for giving us access to the EPR spectrometer, and to C. Lindström for performing many of the experiments. Our thanks are also due to I. Carlsson for much help with the computer program for estimation of the spin-Hamiltonian parameters.

¹D. L. Carter and A. Okaya, *Phys. Rev.* **118**, 1485 (1960).

²M. Ikebe, Y. Miyako, and M. Date, *J. Phys. Soc. Jap.* **26**, 43 (1969).

³Y. Kazumata and Y. Miyako, *J. Phys. Soc. Jap.* **31**, 1727 (1971).

⁴Y. Miyako, *J. Phys. Soc. Jap.* **31**, 1732 (1971).

⁵H. D. Meierling, *Phys. Status Solidi B* **43**, 191 (1971).

⁶E. S. Kirkpatrick, K. A. Müller, and R. A. Rubins, *Phys. Rev.* **135**, A86 (1964).

⁷R. Baer, G. Wessel, and R. S. Rubins, *J. Appl. Phys.* **39**, 23 (1968).

⁸P. O. Andersson, A. Jelenski, and E. Kollberg, Research Report No. 107, Research Laboratory of Electronics and Onsala Space Observatory, Fack, 402 20 Göteborg 5, Sweden (unpublished).

⁹A. E. Siegman, *Microwave Solid State Masers* (McGraw-Hill, New York, 1964).

¹⁰P. O. Andersson, A. Jelenski, and E. Kollberg (unpublished).

¹¹A. Von Hippel, J. Kalnajs, and W. B. Westphal, *J. Phys. Chem. Solids* **23**, 779 (1962).

¹²B. H. Soffer, *J. Chem. Phys.* **35**, 3 (1961), *J. Chem. Phys.* **35**, 940 (1961).

¹³O. W. Johnson, W. D. Ohlsen, and P. I. Kingsbury, Jr., *Phys. Rev.* **175**, 1102 (1968).

¹⁴G. J. Hill, *J. Phys.* **1**, 1151 (1968).

¹⁵G. C. Pimentel and A. L. McClellan, *The Hydrogen Bond* (Freeman, London and San Francisco, 1969).

¹⁶H. L. Schläfer and G. Gliemann, *Einführung in die Liegandfeldtheorie* (Akademische Verlagsgesellschaft, Frankfurt am Main, 1967).